Check for updates

Visible-light-driven photocatalytic degradation of rhodamine B in water by $BiOCl_xI_{1-x}$ solid solutions

Huan-Yan Xu, Dan Lu, Qu Tan, Xiu-Lan He and Shu-Yan Qi

ABSTRACT

Bismuth oxyhalides (BiOXs, X = Cl, Br and I) are emerging photocatalytic materials with unique layered structure, flexible band structure and superior photocatalytic activity. The purpose of this study was to develop a facile alcoholysis route to prepare $BiOCl_xI_{1-x}$ nanosheet solid solutions at room temperature. X-ray diffraction (XRD), field emission scanning electron microscopy (FESEM), transmission electron microscopy (TEM), UV-vis diffuse reflectance spectroscopy (UV-vis DRS), photoluminescence emission spectroscopy (PL) and Brunauer–Emmett–Teller (BET) surface area analyzer were used to characterize the as-prepared photocatalysts. These results revealed that two-dimension $BiOCl_xI_{1-x}$ nanosheet solid solutions could be obtained with high percentage of {001} crystal facets exposed. Moreover, the formation of solid solution could regularly change the optical absorption thresholds and band gaps of $BiOCl_xI_{1-x}$ photocatalysts. The photocatalytic experiments indicated that $BiOCl_{0.75}I_{0.25}$ exhibited the highest photocatalytic performance for the degradation of Rhodamine B (RhB) under simulated sunlight irradiation and the photocatalytic process followed a pseudo-first-order kinetic equation. A possible mechanism of RhB photodegradation over $BiOCl_xI_{1-x}$ solid solutions was proposed based on the structural properties of $BiOCl_xI_{1-x}$ solid solutions and RhB photosensitization.

Key words | alcoholysis, bismuth oxyhalides, photocatalysis, tunable band structure

Huan-Yan Xu (corresponding author)
Dan Lu
Qu Tan
Xiu-Lan He
Shu-Yan Qi
School of Materials Science and Engineering,
Harbin University of Science and Technology,
Harbin 150040,
China
E-mail: *xuhuanyan@hrbust.edu.cn*

INTRODUCTION

Heterogeneous photocatalysis has been widely accepted as an environmentally-benign technology for environmental pollution treatment and renewable energy utilization (Guo *et al.* 2019; Sharma *et al.* 2019; Iervolino *et al.* 2020; Koe *et al.* 2020; Liu *et al.* 2020). The rapid developments of urbanization and industrialization have led to the huge production of wastewater containing organic contaminants. Many methods have been applied for the remediation and treatment of organic wastewater including adsorption, coagulation, extraction, filtration, biodegradation, and advanced oxidation processes (AOPs) (Paździor *et al.* 2019; Pronk *et al.* 2019; Völker *et al.* 2019). Nevertheless, all these methods have some shortcomings as follows: adsorption requires the transportation of target molecules from the aqueous phase to the surface or porous interior of solid phase (Eskandarloo *et al.* 2017); biodegradation takes a long time and is limited to the biodegradable compounds; and large amounts of sludge can be produced in the coagulation process (Kumwimba & Meng 2019). Photocatalysis is considered as a promising technology for the degradation of organic pollutants. Generally, when a photon with enough energy is absorbed by the photocatalyst, the negative electrons in its valence band (VB) are excited and transferred to the conduction band (CB) and the positive holes are accordingly generated in the VB. The holes in VB can react with water (H_2O) or hydroxyl ions (OH^-) to generate hydroxyl radicals (·OH), and the excited electrons in CB can react with oxygen (O_2) to generate superoxide radicals ($\cdot O_2^-$). These radicals subsequently take part in the redox reactions and lead to the complete mineralization of pollutant molecules by their degradation into H_2O and CO_2 (Khaki *et al.* 2017; MiarAlipour *et al.* 2018). In recent decades, various semiconductor materials and their heterojunctions, such as TiO_2 (Meng *et al.* 2019), TiO_2/CdS (Low *et al.* 2019), ZnO/CdS (Wang *et al.* 2019a), WO_3/g-C_3N_4 (Fu *et al.* 2019), MoS_2/g-C_3N_4 (Yuan *et al.* 2019) and TaON/V_2O_5 (Wang *et al.* 2019b), have been developed as effective photocatalysts triggered by UV or visible light. Furthermore, recent developments in Bi-based semiconductors have heightened the need for photocatalysis in

doi: 10.2166/wst.2020.205

Downloaded from http://iwaponline.com/wst/article-pdf/81/5/1080/768292/wst081051080.pdf
by guest

relation to appropriate band gap for visible-light response and hybridized valence band composed of Bi 6s and O 2p orbitals (Meng & Zhang 2016; Li *et al.* 2018).

Bismuth oxyhalides (BiOXs, X = Cl, Br and I) have been considered as the most promising candidates as photocatalytic materials since the unique layered structure endows them with flexible band structure and superior photocatalytic activity (Li *et al.* 2014a; Bhachu *et al.* 2016). The typical layered structure of BiOXs is constructed by $[Bi_2O_2]^{2+}$ layers intercalated with $[X]^-$ between the layers. The atoms within $[Bi_2O_2]^{2+}$ layers interact with each other via covalent bonds, whereas the stack along the *c*-axis of [X] layers is bonded by van der Waals force. Thereby, the sandwich-like layered structures are configured by the intralayer covalent bonding and interlayer van der Waals interaction (Li *et al.* 2014a; Xu *et al.* 2016). Moreover, the internal electric field (IEF) along *c*-axis can be generated in BiOX structure, attributed to the asymmetry of charge distribution between $[Bi_2O_2]^{2+}$ and $[X]^-$ layers (Li *et al.* 2014a). IEF can efficiently separate the photogenerated electron-hole pairs and prevent their recombinations (Li *et al.* 2017). However, previously published reports indicated that the photocatalytic efficiency of pristine BiOX was not high enough for practical use. Many modification attempts, such as doping by noble metals, morphology modulation, composition design and combination with other materials, have been made to improve the photocatalytic activity of pure BiOX (Bielicka-Giełdoń *et al.* 2019; Sharma *et al.* 2019; Wang *et al.* 2019c). Among BiOXs, the band gaps of BiOCl, BiOBr and BiOI were found to be 3.22, 2.64, and 1.77 eV, respectively (Ren *et al.* 2013). Therefore, BiOCl and BiOBr can be mainly excited by UV light, while BiOI can respond to visible light. Nevertheless, BiOI still exhibits poor photo-catalytic property because of its low quantum efficiency, weak photo-oxidation ability and easy recombination of photogenerated electrons and holes (Hou *et al.* 2017). It has been reported that, when iodine was introduced into BiOCl; or chlorine into BiOI, dramatic increases in photo-catalytic performance could be observed under visible light irradiation (Kim *et al.* 2014; Tian *et al.* 2016). Since BiOXs have the same layered structure and atomic configuration, it is very easy to realize the substitution of halogen atoms to form $BiOX_xY_{1-x}$ (X, Y = Cl, Br and I) solid solutions with unlimited solubility (Keller & Krämer 2005). Previous studies have demonstrated that the formation of solid solutions could substantially modulate the band gap and improve visible-light photocatalytic activity of BiOXs (Zhang *et al.* 2015, 2016; Yang *et al.* 2016). We have developed a facile alcoholysis route to successfully synthesize $BiOCl_xBr_{1-x}$ and $BiOBr_xI_{1-x}$ solid solutions and found that they exhibited higher photocatalytic performance under visible-light irradiation (Xu *et al.* 2017a, 2017b).

These findings encouraged us to go ahead and attempt the synthesis of $BiOCl_xI_{1-x}$ solid solutions through the alcoholysis method in this work. The obtained photocatalysts were characterized by X-ray diffraction (XRD), field emission scanning electron microscopy (FESEM), transmission electron microscopy (TEM), UV-vis diffuse reflectance spectroscopy (UV-vis DRS), photoluminescence emission spectroscopy (PL) and Brunauer–Emmett–Teller (BET) surface area analysis. Then, the active dye Rhodamine B (RhB) was employed as the targeted contaminant to evaluate the photocatalytic performance of these photocatalysts under simulated sunlight irradiation. Finally, the possible photocatalytic mechanism was proposed and discussed.

EXPERIMENTAL SECTION

Preparation of $BiOCl_xI_{1-x}$ solid solutions

A facile alcoholysis method was used to prepare $BiOCl_xI_{1-x}$ nanosheet solid solutions at room temperature and atmospheric pressure. All the chemical reagents were of analytical grade and were used without further purification. $Bi(NO_3)_3{\cdot}5H_2O$, KCl and KI were employed as Bi, Cl and I sources, respectively. In a typical alcoholysis route, according to the stoichiometric value of x ($x = 1.0$, 0.75, 0.5, 0.25, and 0.0 for this study) in $BiOCl_xI_{1-x}$ solid solutions, stoichiometric amounts of KCl and KI were first dissolved in as little deionized water as possible. After the above first step, requisite amounts of $Bi(NO_3)_3{\cdot}5H_2O$ and absolute ethyl alcohol were successively put into a 200 mL beaker and the process of alcoholysis was started by ultrasonic irradiation until $Bi(NO_3)_3{\cdot}5H_2O$ was completely dissolved in absolute ethyl alcohol. Subsequently, the KCl-KI mixed solution prepared in the first step was added to the above obtained alcoholysate and the mixture was mechanically stirred for 6 h. Then, the suspension was centrifuged to separate the solid product from solution. The resulting solid was washed by deionized water and absolute ethyl alcohol alternately until the filtrate reached neutral pH. After filtration, the resulting solid was dried at 80 °C for 6 h followed by grinding to obtain the powder of $BiOCl_xI_{1-x}$ solid solutions for subsequent studies.

Characterization methods

XRD was employed to identify the crystal phase of as-prepared photocatalysts by a PANalytical X'Pert X-ray

Downloaded from http://iwaponline.com/wst/article-pdf/81/5/1080/768292/wst081051080.pdf
by guest

diffractometer with Cu-K_α radiation ($\lambda = 0.15418$ nm) over the 2θ range of 5°–80°. Based on 2θ values in XRD patterns, the lattice parameters of $BiOCl_xI_{1-x}$ solid solutions were calculated by UnitCell software. The interlayer spacing of (001) crystal plane was calculated by the Bragg's equation ($\lambda = 2d\sin\theta$). FESEM and TEM were used to observe the microscopic morphology of $BiOCl_xI_{1-x}$ solid solutions, operated on FEISirion200 scanning electron microscope and JEOL JEM 2010 transmission electron microscope, respectively. The changes of optical absorption and band gap for $BiOCl_xI_{1-x}$ solid solutions were investigated by UV-vis DRS spectra. They were obtained on an USB4000 UV-vis spectrometer with an integral sphere (Ocean Optics) and a standard template bought from South Africa Optics was used as the reference. PL spectra were collected by a RF-5301PC fluorescence spectrophotometer at room temperature. A 150 W Xenon lamp was used as the excitation light source ($\lambda_{ex} = 304$ nm). PL spectra were helpful to gain the detailed information of the recombination of photogenerated electron-hole pairs. At the liquid nitrogen temperature, BET specific surface area of $BiOCl_xI_{1-x}$ photocatalysts was measured on a Sibata SA-1100 surface area analyzer based on nitrogen adsorption–desorption data.

Photocatalytic tests

In the photocatalytic process, a 100 $mW{\cdot}cm^{-2}$ Xe lamp was used as the simulated solar light. 100 mg of $BiOCl_xI_{1-x}$ photocatalyst was added into 100 mL RhB solution, whose initial concentration (C_0) was 20 $mg{\cdot}L^{-1}$. Before turning on the Xe lamp, the suspension was magnetically stirred in the dark for 60 min to balance the adsorption and desorption. Afterwards, the Xe lamp was turned on and photocatalytic reaction started under continuous stirring. At regular 30 min intervals, about 5 mL of the suspension was extracted from the reaction liquid and the supernatant was obtained by centrifugation. The residual RhB concentration (C) in the supernatant was detected by 751II UV-vis spectrophotometer at RhB maximum absorption wavelength (553 nm). And, UV-vis absorption spectra were employed to analyze the residual RhB solutions after different photocatalytic periods.

RESULTS AND DISCUSSION

Characterization of $BiOCl_xI_{1-x}$ solid solutions

Figure 1 provides the XRD results of $BiOCl_xI_{1-x}$ solid solutions. All the sharp diffraction peaks in the figure

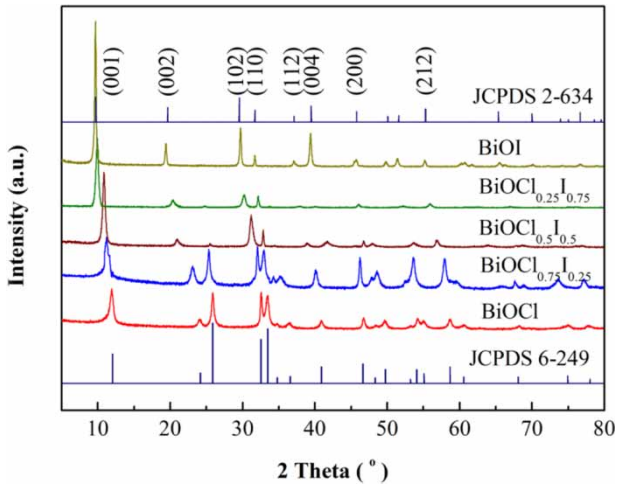

Figure 1 | XRD patterns of $BiOCl_xI_{1-x}$ solid solutions prepared by alcoholysis route.

indicated that $BiOCl_xI_{1-x}$ photocatalysts prepared by the alcoholysis route were well crystallized (Lei *et al.* 2009). The end-members BiOCl and BiOI seem to be consistent with JCPDS 6-249 and JCPDS 2-634, respectively. It should be noted that, as the x value in $BiOCl_xI_{1-x}$ decreases, all the diffraction peaks are expected to show a regular shift to the small angle region. This finding can be interpreted by the fact that, when the smaller Cl atoms ($r_{Cl} = 0.181$ nm) are replaced by larger I atoms ($r_I = 0.216$ nm), the interlayer spacing of the crystal structure expands. In addition, when the x value decreases, the lattice parameters a and c of $BiOCl_xI_{1-x}$ solid solutions gradually increased, as listed in Table 1. These regular changes in XRD peak positions and lattice parameters strongly suggested that a group of $BiOCl_xI_{1-x}$ solid solutions was obtained (Xu *et al.* 2017a 2017b). Moreover, no other diffraction peaks of impurity phases could be seen in the XRD patterns, suggesting that perhaps all the atoms have entered into the crystal lattice and the stoichiometric value x in $BiOCl_xI_{1-x}$ can be accurately determined by the initial proportion of Cl and I sources in the preparation procedure (Yang *et al.* 2016). From Figure 1,

Table 1 | Lattice parameter, BET surface area, band gap and (001) interlayer spacing (d_{001}) of $BiOCl_xI_{1-x}$ solid solutions

	$a = b$ (nm)	c (nm)	S_{BET} ($m^2{\cdot}g^{-1}$)	E_g (eV)	d_{001} (nm)
BiOCl	0.3888	0.7381	5.39	3.28	0.7437
$BiOCl_{0.75}I_{0.25}$	0.3902	0.7529	7.73	2.08	0.7900
$BiOCl_{0.5}I_{0.5}$	0.3946	0.8108	7.16	2.04	0.8192
$BiOCl_{0.25}I_{0.75}$	0.3976	0.8560	6.85	2.01	0.8934
BiOI	0.4012	0.9133	6.22	1.86	0.9137

Downloaded from http://iwaponline.com/wst/article-pdf/81/5/1080/768292/wst081051080.pdf
by guest

it can also be observed that the (001) peak exhibits the strongest diffraction intensity in all the XRD patterns, indicating that the exposure percentage of {001} crystal plane is rather higher in $BiOCl_xI_{1-x}$ solid solutions compared to pure BiOCl. This phenomenon might be attributed to the highly preferred (001) orientation (Li *et al.* 2014b). Therefore, it might be determined that the as-obtained photocatalysts in this study were $BiOCl_xI_{1-x}$ solid solutions with high exposure of {001} crystal plane.

Through the FESEM images of $BiOCl_{0.75}I_{0.25}$, $BiOCl_{0.5}I_{0.5}$ and $BiOCl_{0.25}I_{0.75}$ (Figure 2), we can observe that all the $BiOCl_xI_{1-x}$ photocatalysts exhibit two-dimension flake-like shape with the diameter of 0.2–1.0 μm. These nanoplates were stacked together irregularly without any specific architecture such as microspheres or flowers. In TEM images (Figure 3(a)–3(e)), the overlayed shadow of two-dimension $BiOCl_xI_{1-x}$ nanosheets can be clearly seen. Moreover, the wrinkles of nanosheets can be obviously seen as well, which might result from the inner strain in $BiOCl_xI_{1-x}$ structure. The existence of inner strain can change the electronic band structure and quicken the electron-hole separation, which could correspondingly improve the photocatalytic activity of BiOXs (Feng *et al.* 2015). The pattern of selected area electron diffraction (SAED) of $BiOCl_{0.5}I_{0.5}$ (Figure 3(f)) shows a group of diffraction rings, indicating the polycrystalline character of $BiOCl_{0.5}I_{0.5}$. The indices of crystal plane corresponding to diffraction rings are given in the pattern.

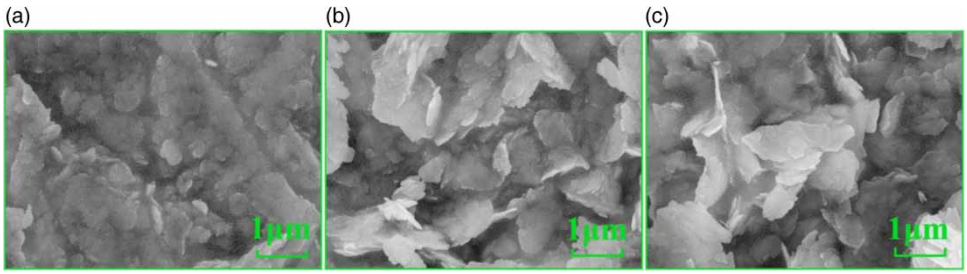

Figure 2 | FESEM images of (a) $BiOCl_{0.75}I_{0.25}$, (b) $BiOCl_{0.5}I_{0.5}$ and (c) $BiOCl_{0.25}I_{0.75}$.

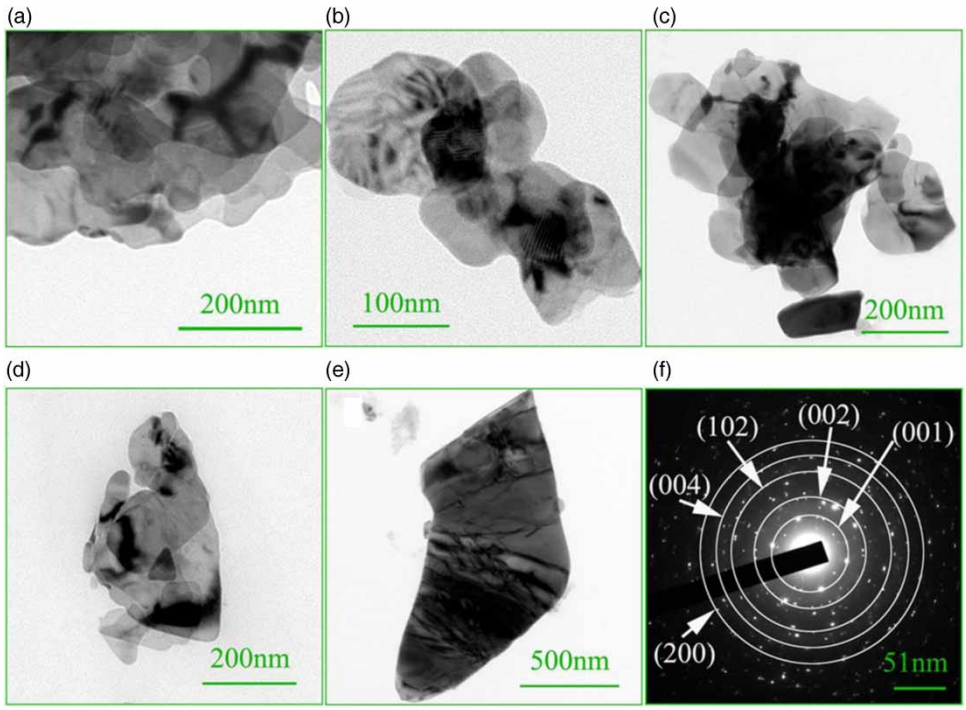

Figure 3 | TEM images of (a) BiOCl, (b) $BiOCl_{0.75}I_{0.25}$, (c) $BiOCl_{0.5}I_{0.5}$, (d) $BiOCl_{0.25}I_{0.75}$ and (e) BiOI; (f) SAED pattern of $BiOCl_{0.5}I_{0.5}$.

Downloaded from http://iwaponline.com/wst/article-pdf/81/5/1080/768292/wst081051080.pdf
by guest

Figure 4(a) illustrates the UV-vis DRS spectra of $BiOCl_xI_{1-x}$ solid solutions. It can be seen that the optical absorption thresholds of BiOCl and BiOI correspond to 391.7 and 672.8 nm, respectively, suggesting that BiOCl can be excited only by UV light while BiOI can respond to visible light. The optical absorption thresholds of the other three $BiOCl_xI_{1-x}$ solid solutions are expected to be present between those of BiOCl and BiOI, and systematically increase with increasing I content. Furthermore, the color of $BiOCl_xI_{1-x}$ solid solutions gradually changed from milky white of BiOCl to reddish brown of BiOI. The band gap (E_g) of $BiOCl_xI_{1-x}$ solid solutions can be determined according to UV-vis DRS spectra, as shown in Figure 4(b) and Table 1. Interestingly, the E_g values of $BiOCl_xI_{1-x}$ photocatalysts gradually decrease with I content increasing. This also indicates the formation of $BiOCl_xI_{1-x}$ solid solutions. Judging from the regular change of E_g values, it can be strongly inferred that the band structure of $BiOCl_xI_{1-x}$ solid solutions can be modulated by the substitution of smaller Cl ions by larger I ions. It has been proved previously that, for BiOX semiconductors, the conduction band minimum (CBM) is contributed by Bi 6p orbitals and the valence band maximum (VBM) is dominated by O 2p and X *n*p orbitals ($n = 3$, 4 and 5 for X = Cl, Br and I, respectively) (Li *et al.* 2014a; Xu *et al.* 2016). Therefore, as I content increased, the contribution of I 5p orbitals dramatically increased and band gap of $BiOCl_xI_{1-x}$ photocatalysts decreased.

Photocatalytic performance of $BiOCl_xI_{1-x}$ solid solutions

Figure 5(a) depicts the photocatalytic degradation of RhB in aqueous solution by $BiOCl_xI_{1-x}$ photocatalysts under simulated sunlight irradiation. As known, the adsorption played

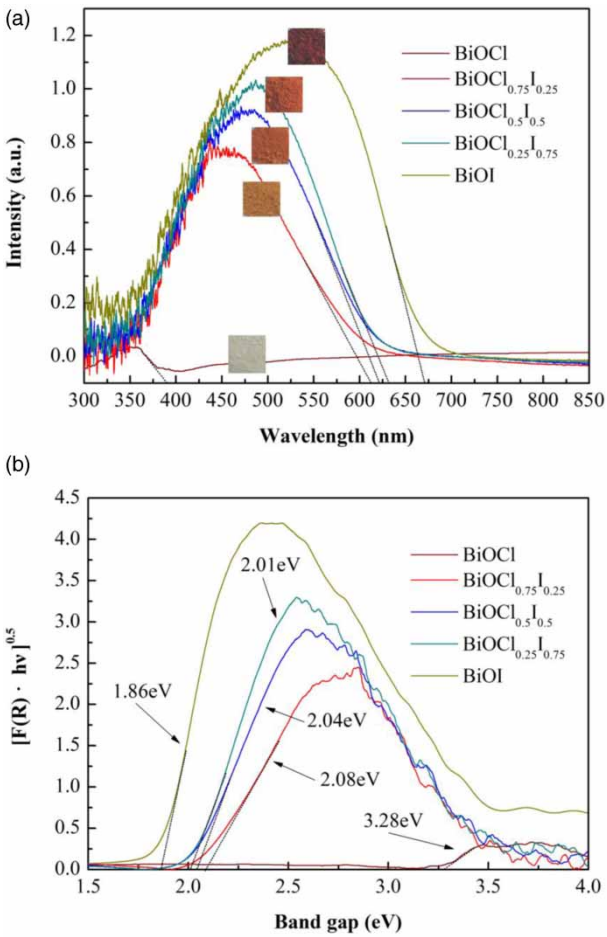

Figure 4 | (a) UV-vis DRS spectra and the change in color of $BiOCl_xI_{1-x}$ solid solutions; (b) relationships between $[F(R)\cdot h\upsilon]^{0.5}$ and band gap.

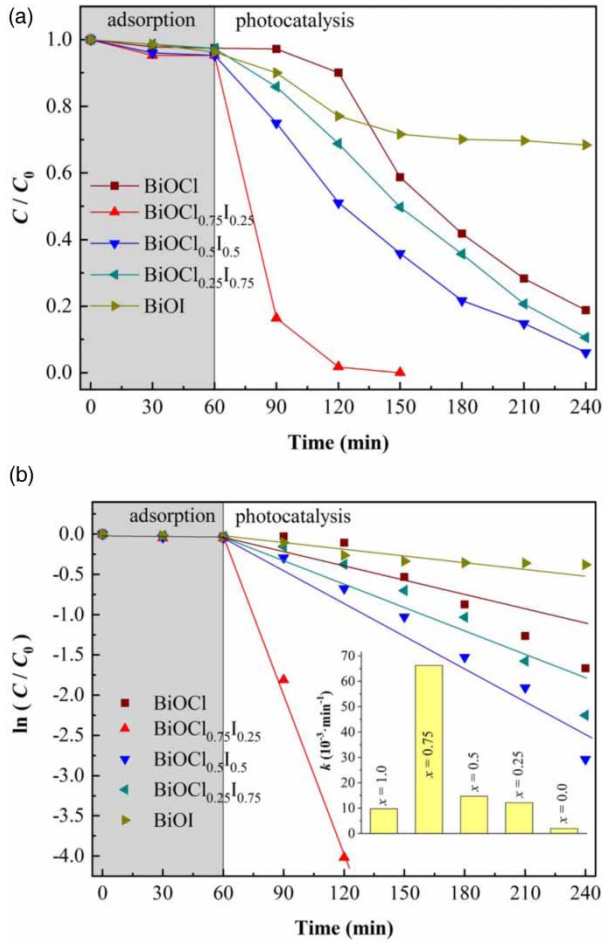

Figure 5 | (a) Photocatalytic degradation of RhB over $BiOCl_xI_{1-x}$ photocatalysts under simulated sunlight irradiation; (b) pseudo-first-order kinetic curves of RhB photodegradation processes (Inset: reaction rate constants for different photocatalysts).

Downloaded from http://iwaponline.com/wst/article-pdf/81/5/1080/768292/wst081051080.pdf
by guest

an important part in the heterogeneous photocatalytic reactions. In this study, when the adsorption and desorption reached equilibrium, the adsorbed amounts of RhB onto $BiOCl_xI_{1-x}$ photocatalysts with different x values were almost similar. This might be attributed to the fact that the photocatalysts had no distinct difference in their surface areas (see Table 1). We can also find from this figure that $BiOCl_{0.75}I_{0.25}$, $BiOCl_{0.5}I_{0.5}$ and $BiOCl_{0.25}I_{0.75}$ exhibited better photocatalytic activity than BiOCl and BiOI. Only 31.5% and 81.2% of RhB could be degraded over BiOI and BiOCl, respectively, within 240 min of reaction time; nevertheless, almost all the RhB could be degraded over $BiOCl_{0.75}I_{0.25}$ within 150 min reaction time. Because the adsorption had little effect on photocatalytic evaluation, the enhanced photocatalytic activity of $BiOCl_{0.75}I_{0.25}$, $BiOCl_{0.5}I_{0.5}$ and $BiOCl_{0.25}I_{0.75}$ didn't essentially depend on adsorption. Among $BiOCl_xI_{1-x}$ solid solutions, $BiOCl_{0.75}I_{0.25}$ had the highest photocatalytic activity, in accordance with the previous report (Ren *et al.* 2013).

In addition, Figure 5(b) reveals that the photocatalytic degradation of RhB in aqueous solution follows a pseudo-first-order kinetic model [$\ln(C/C_0) = kt$]. The reaction rate constants are calculated and illustrated in the inset of Figure 5(b). The k values of $BiOCl_{0.75}I_{0.25}$, $BiOCl_{0.5}I_{0.5}$ and $BiOCl_{0.25}I_{0.75}$ are approximately 34.1, 7.58 and 6.24 times higher, respectively, than that of BiOI; and approximately 6.82, 1.51 and 1.24 times higher, respectively, than that of BiOCl, strongly suggesting the enhanced photocatalytic activity of $BiOCl_xI_{1-x}$ solid solutions.

When $BiOCl_{0.75}I_{0.25}$ was used as the photocatalyst, UV-vis absorption spectra of RhB solution after different photodegradation periods were analyzed. Figure 6(a) demonstrates that, as the photocatalytic reaction progressed, the UV-vis absorption peaks of RhB solution gradually weakened and even disappeared. This result infers that almost all the RhB molecules were decomposed into the substances with small molecular weight. Furthermore, the stability is equally important for a photocatalyst. We also use $BiOCl_{0.75}I_{0.25}$ as the representative sample to evaluate the recyclability of $BiOCl_xI_{1-x}$ solid solution photocatalysts. Figure 6(b) reveals that, even after four runs, $BiOCl_{0.75}I_{0.25}$ still has high photocatalytic activity. This suggests that $BiOCl_xI_{1-x}$ solid solutions not only exhibited high photocatalytic activity but also showed excellent photocatalytic stability.

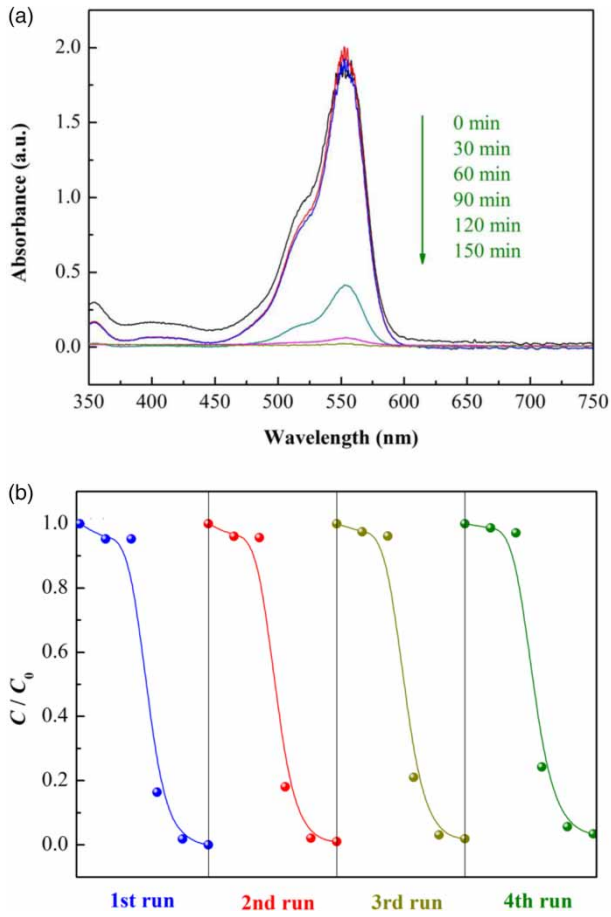

Figure 6 | (a) UV-vis absorption spectra of RhB solution after different photodegradation periods and (b) cycling tests on RhB photodegradation over $BiOCl_{0.75}I_{0.25}$.

Possible photocatalytic mechanism

In our previous studies, it has been found that the photocatalytic properties of BiOXs solid solutions were closely dependent on the IEF, electronic band structure and interlayer spacing of (001) crystal plane (d_{001}) (Xu *et al.* 2017a 2017b). Stronger IEF could promote electron-hole pairs transfer and inhibit their recombination, accordingly resulting in higher photocatalytic activity of {001} facet-dominant BiOX nanosheets (Li *et al.* 2014a). On the other hand, the increased d_{001} might augment the transfer distance of photogenerated charge driven by IEF, suppressing the effective electron-hole separation and thereby decreasing the photocatalytic ability of $BiOCl_xI_{1-x}$ photocatalysts. Based on XRD results and Bragg's equation ($\lambda = 2d\sin\theta$), the interlayer spacing d_{001} of $BiOCl_xI_{1-x}$ samples was calculated and listed in Table 1. It can be obviously seen that the (001) interlayer spacing gradually increases with the increase of I content in $BiOCl_xI_{1-x}$ photocatalysts. This means that the electron-hole separation efficiency might be suppressed when I content increases. PL spectrum was employed to analyze the separation efficiency of photogenerated electron-hole pairs in $BiOCl_xI_{1-x}$ photocatalysts and the results are presented in Figure 7. We can find that BiOCl has

Downloaded from http://iwaponline.com/wst/article-pdf/81/5/1080/768292/wst081051080.pdf
by guest

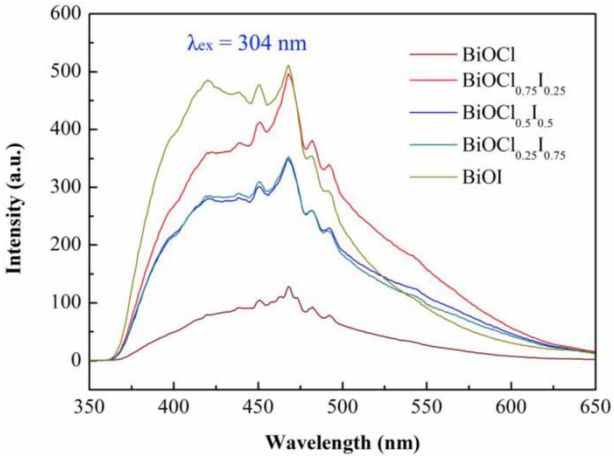

Figure 7 | PL spectra of $BiOCl_xI_{1-x}$ solid solutions.

the best separation efficiency of electron-hole pairs among these photocatalysts. Whereas, the PL peak intensity of BiOI is the strongest, implying that the electron-hole pairs in BiOI tend to recombine (Jiang *et al.* 2012). For the other three $BiOCl_xI_{1-x}$ photocatalysts, the electron-hole separation efficiency seems not in positive correlation with the interlayer spacing of (001) crystal plane. This might be ascribed to the difference in IEF magnitudes of these three photocatalysts. Hence, it can be inferred that the separation efficiency of electron-hole pairs in $BiOCl_xI_{1-x}$ is determined by the synergy between (001) interlayer spacing and IEF magnitude.

In addition, different molar ratios of Cl and I in $BiOCl_xI_{1-x}$ solid solutions would generate different energy levels of hybrid orbitals, which means that the electronic band structure of $BiOCl_xI_{1-x}$ can be modulated by the alteration of x value in $BiOCl_xI_{1-x}$. As shown in Figure 4(b) and Table 1, the E_g values of $BiOCl_xI_{1-x}$ photocatalysts successively decrease with the increase of I content. Hence, as I content increased, $BiOCl_xI_{1-x}$ photocatalysts were more easily excited by visible light and exhibited higher photocatalytic activity. As discussed above (Figure 5(a)), $BiOCl_{0.75}I_{0.25}$, $BiOCl_{0.5}I_{0.5}$ and $BiOCl_{0.25}I_{0.75}$ showed better photocatalytic activity than BiOCl and BiOI. Because BiOCl had the widest band gap (3.28 eV) among $BiOCl_xI_{1-x}$ photocatalysts, it could not be effectively triggered by visible light. While, for BiOI, its separation efficiency of electron-hole pairs was the worst among these photocatalysts. Therefore, the visible-light-driven photocatalytic activities of BiOCl and BiOI were much lower than those of $BiOCl_{0.75}I_{0.25}$, $BiOCl_{0.5}I_{0.5}$ and $BiOCl_{0.25}I_{0.75}$. Based on the above discussions, the possible mechanism of RhB photodegradation over $BiOCl_xI_{1-x}$ solid solutions triggered by visible light was proposed. As shown in Figure 8, when $BiOCl_xI_{1-x}$ semiconductor is irradiated by simulated solar light, the electrons (e^-) are excited to the conduction band and the holes (h^+) are generated in the valence band. However, the electron-hole pairs tend to recombine to reduce total energy of the system, thereby resulting in the decrease of photocatalytic ability. In $BiOCl_xI_{1-x}$ semiconductor, IEF can drive the electrons and holes to $[Bi_2O_2]^{2+}$ and $[X]^-$ layers, respectively, realizing their effective separation. But, larger interlayer spacing of (001) crystal plane can lead to a longer distance between $[Bi_2O_2]^{2+}$ and $[X]^-$ layers, which would be not helpful to the separation of photogenerated charges. Therefore, the photocatalytic performance of $BiOCl_xI_{1-x}$ solid solutions is simultaneously affected by these structural factors. In addition, it has been verified that there existed a strong interaction between RhB and BiOX nanosheets, which could facilitate the electron injection from excited RhB* into conduction band of BiOX nanosheets (Hu *et al.* 2014). The matching energy levels of excited RhB* and BiOX nanosheets also played a crucial role in the

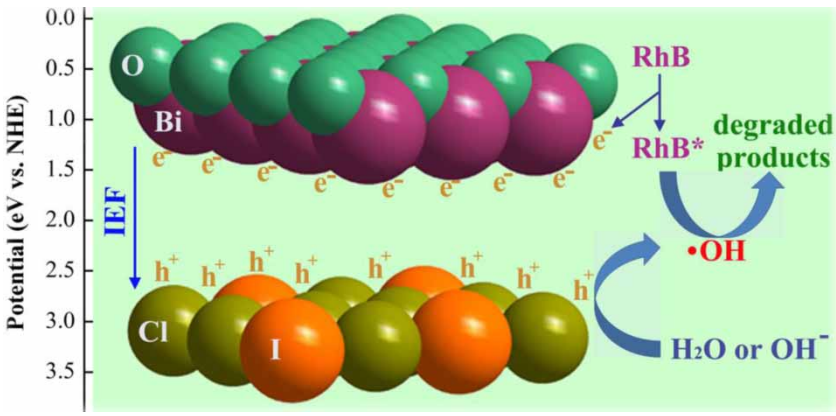

Figure 8 | Possible mechanism of RhB photodegradation over $BiOCl_xI_{1-x}$ solid solutions.

Downloaded from http://iwaponline.com/wst/article-pdf/81/5/1080/768292/wst081051080.pdf
by guest

photosensitization process (Zhang *et al.* 2015; Chen *et al.* 2016). The photosensitization of RhB helps with its photodegradation.

CONCLUSIONS

A facile alcoholysis method was successfully used to prepare $BiOCl_xI_{1-x}$ solid solutions at room temperature and atmospheric pressure. The regular changes in XRD peak positions and cell parameters strongly suggested that the obtained products belong to a group of solid solutions. The strong diffraction intensity of (001) peak indicated the high exposure percentage of {001} crystal facets in $BiOCl_xI_{1-x}$ solid solutions. Two-dimensional $BiOCl_xI_{1-x}$ nanosheets could be clearly observed by FESEM and TEM. The optical absorption threshold of $BiOCl_xI_{1-x}$ solid solutions proportionately increased with increasing I content, accordingly their band gaps gradually decreased, suggesting that the formation of solid solution could modify the optical absorption property and band structure of BiOX. $BiOCl_{0.75}I_{0.25}$, $BiOCl_{0.5}I_{0.5}$ and $BiOCl_{0.25}I_{0.75}$ exhibited higher photocatalytic activity than BiOCl and BiOI. Among all the $BiOCl_xI_{1-x}$ photocatalysts, $BiOCl_{0.75}I_{0.25}$ had the highest photocatalytic activity. Moreover, the RhB photodegradation processes over $BiOCl_xI_{1-x}$ followed a pseudo-first-order kinetic equation. $BiOCl_xI_{1-x}$ solid solutions not only had high photocatalytic activity but also showed excellent photocatalytic stability. The IEF, electronic band structure and interlayer spacing of (001) crystal plane were the important structural factors that affected the photocatalytic performance of $BiOCl_xI_{1-x}$ solid solutions. Furthermore, the photosensitization of RhB also played a crucial role in its photodegradation. Towards practical applications of $BiOCl_xI_{1-x}$ photocatalysts, future research should be put on the photocatalyst separation and solar-reactor designs. Many methods such as centrifugation, flocculation, flotation, membrane technology or their combinations seem to show great potentials for the separation of nanoscale photocatalysts from their aqueous suspensions. Moreover, magnetic separation is also considered to be an alternative strategy when a core-shell heterojunction is fabricated using a magnetic material like Fe_3O_4 and $BiOCl_xI_{1-x}$ nanosheets as the core and shell, respectively. On the other hand, the solar-to-chemical efficiency might be the most important indicator for the photocatalytic reactor designs. To gain higher efficiency, light absorption, heat and mass transfer, and reaction kinetics must be further investigated. In addition, the optimizations of operating condition and geometric configuration are equally indispensable for the design of a high-efficiency reactor.

REFERENCES

Bhachu, D. S., Moniz, S. J., Sathasivam, S., Scanlon, D. O., Walsh, A., Bawaked, S. M., Mokhtar, M., Obaid, A. Y., Parkin, I. P., Tang, J. W. & Carmalt, C. J. 2016 Bismuth oxyhalides: synthesis, structure and photoelectrochemical activity. *Chemical Science* **7**, 4832–4841.

Bielicka-Giełdoń, A., Wilczewska, P., Malankowska, A., Szczodrowski, K., Ryl, J., Zielińska-Jurek, A. & Siedlecka, E. M. 2019 Morphology, surface properties and photocatalytic activity of the bismuth oxyhalides semiconductors prepared by ionic liquid assisted solvothermal method. *Separation and Purification Technology* **217**, 164–173.

Chen, H. B., Yu, X., Zhu, Y., Fu, X. H. & Zhang, Y. M. 2016 Controlled synthesis of {001} facets-dominated dye-sensitized BiOCl with high photocatalytic efficiency under visible-light irradiation. *Journal of Nanoparticle Research* **18**, 225.

Eskandarloo, H., Kierulf, A. & Abbaspourrad, A. 2017 Nano- and micromotors for cleaning polluted waters: focused review on pollutant removal mechanisms. *Nanoscale* **9**, 13850–13863.

Feng, H. F., Xu, Z. F., Wang, L., Yu, Y. X., Mitchell, D., Cui, D. D., Xu, X., Shi, J., Sannomiya, T., Du, Y., Hao, W. C. & Dou, S. X. 2015 Modulation of photocatalytic properties by strain in 2D BiOBr nanosheets. *ACS Applied Materials & Interfaces* **7**, 27592–27596.

Fu, J., Xu, Q., Low, J., Jiang, C. & Yu, J. 2019 Ultrathin 2D/2D WO_3/g-C_3N_4 step-scheme H_2-production photocatalyst. *Applied Catalysis B-Environmental* **243**, 556–565.

Guo, Q., Ma, Z., Zhou, C., Ren, Z. & Yang, X. 2019 Single molecule photocatalysis on TiO_2 surfaces. *Chemical Reviews* **119**, 11020–11041.

Hou, J. H., Jiang, K., Shen, M., Wei, R., Wu, X. G., Idrees, F. & Cao, C. B. 2017 Micro and nano hierachical structures of BiOI/activated carbon for efficient visible-light-photocatalytic reactions. *Scientific Reports* **7**, 11665.

Hu, J. L., Fan, W. J., Ye, W. Q., Huang, C. J. & Qiu, X. Q. 2014 Insights into the photosensitivity activity of BiOCl under visible light irradiation. *Applied Catalysis B-Environmental* **158–159**, 182–189.

Iervolino, G., Zammit, I., Vaiano, V. & Rizzo, L. 2020 Limitations and prospects for wastewater treatment by UV and visible-light-active heterogeneous photocatalysis: a critical review. *Topics in Current Chemistry* **378**, 7.

Jiang, J., Zhao, K., Xiao, X. Y. & Zhang, L. Z. 2012 Synthesis and facet-dependent photoreactivity of BiOCl single-crystalline nanosheets. *Journal of the American Chemical Society* **134**, 4473–4476.

Keller, E. & Krämer, V. 2005 A strong deviation from Vegard's rule: X-ray powder investigations of the three quasi-binary phase systems BiOX-BiOY (X, Y = Cl, Br, I). *Zeitschrift für Naturforschung B* **60**, 1255–1263.

Downloaded from http://iwaponline.com/wst/article-pdf/81/5/1080/768292/wst081051080.pdf
by guest

Khaki, M. R. D., Shafeeyan, M. S., Raman, A. A. A. & Daud, W. M. A. W. 2017 Application of doped photocatalysts for organic pollutant degradation – a review. *Journal of Environmental Management* **198**, 78–94.

Kim, W. J., Pradhan, D., Min, B.-K. & Sohn, Y. 2014 Adsorption/photocatalytic activity and fundamental natures of BiOCl and $BiOCl_xI_{1-x}$ prepared in water and ethylene glycol environments, and Ag and Au-doping effects. *Applied Catalysis B-Environmental* **147**, 711–725.

Koe, W. S., Lee, J. W., Chong, W. C., Pang, Y. L. & Sim, L. C. 2020 An overview of photocatalytic degradation: photocatalysts, mechanisms, and development of photocatalytic membrane. *Environmental Science and Pollution Research* **27**, 2522–2565.

Kumwimba, M. N. & Meng, F. 2019 Roles of ammonia-oxidizing bacteria in improving metabolism and cometabolism of trace organic chemicals in biological wastewater treatment processes: a review. *Science of the Total Environment* **659**, 419–441.

Lei, Y. Q., Wang, G. H., Song, S. Y., Fan, W. Q. & Zhang, H. J. 2009 Synthesis, characterization and assembly of BiOCl nanostructure and their photocatalytic properties. *CrystEngComm* **11**, 1857–1862.

Li, J., Yu, Y. & Zhang, L. Z. 2014a Bismuth oxyhalide nanomaterials: layered structures meet photocatalysis. *Nanoscale* **6**, 8473–8488.

Li, H., Shi, J. G., Zhao, K. & Zhang, L. Z. 2014b Sustainable molecular oxygen activation with oxygen vacancies on the {001} facets of BiOCl nanosheets under solar light. *Nanoscale* **6**, 14168–14173.

Li, J., Li, H., Zhan, G. M. & Zhang, L. Z. 2017 Solar water splitting and nitrogen fixation with layered bismuth oxyhalides. *Accounts of Chemical Research* **50**, 112–121.

Li, M., Huang, H., Yu, S., Tian, N. & Zhang, Y. 2018 Facet, junction and electric field engineering of bismuth-based materials for photocatalysis. *ChemCatChem* **10**, 4477–4496.

Liu, Y., Huang, D., Cheng, M., Liu, Z., Lai, C., Zhang, C., Zhou, C., Xiong, W., Qin, L., Shao, B. & Liang, Q. 2020 Metal sulfide/MOF-based composites as visible-light-driven photocatalysts for enhanced hydrogen production from water splitting. *Coordination Chemistry Reviews* **409**, 213220.

Low, J., Dai, B., Tong, T., Jiang, C. & Yu, J. 2019 In situ irradiated X-ray photoelectron spectroscopy investigation on a direct Z-scheme TiO_2/CdS composite film photocatalyst. *Advanced Materials* **31**, 1802981.

Meng, X. & Zhang, Z. 2016 Bismuth-based photocatalytic semiconductors: introduction, challenges and possible approaches. *Journal of Molecular Catalysis A-Chemical* **423**, 533–549.

Meng, A., Zhang, L., Cheng, B. & Yu, J. 2019 Dual cocatalysts in TiO_2 photocatalysis. *Advanced Materials* **31**, 1807660.

MiarAlipour, S., Friedmann, D., Scott, J. & Amal, R. 2018 Tio_2/porous adsorbents: recent advances and novel applications. *Journal of Hazardous Materials* **341**, 404–423.

Paździor, K., Bilińska, L. & Ledakowicz, S. 2019 A review of the existing and emerging technologies in the combination of AOPs and biological processes in industrial textile wastewater treatment. *Chemical Engineering Journal* **376**, 120597.

Pronk, W., Ding, A., Morgenroth, E., Derlon, N., Desmond, P., Burkhardt, M., Wu, B. & Fane, A. G. 2019 Gravity-driven membrane filtration for water and wastewater treatment: a review. *Water Research* **149**, 553–565.

Ren, K. X., Liu, J., Liang, J., Zhang, K., Zheng, X., Luo, H. D., Huang, Y. B., Liu, P. J. & Yu, X. B. 2013 Synthesis of the bismuth oxyhalide solid solutions with tunable band gap and photocatalytic activities. *Dalton Transactions* **42**, 9706–9712.

Sharma, K., Dutta, V., Sharma, S., Raizada, P., Hosseini-Bandegharaei, A., Thakur, P. & Singh, P. 2019 Recent advances in enhanced photocatalytic activity of bismuth oxyhalides for efficient photocatalysis of organic pollutants in water: a review. *Journal of Industrial and Engineering Chemistry* **78**, 1–20.

Tian, F., Zhao, H. P., Dai, Z., Cheng, G. & Chen, R. 2016 Mediation of valence band maximum of BiOI by Cl incorporation for improved oxidation power in photocatalysis. *Industrial & Engineering Chemistry Research* **55**, 4969–4978.

Völker, J., Stapf, M., Miehe, U. & Wagner, M. 2019 Systematic review of toxicity removal by advanced wastewater treatment technologies via ozonation and activated carbon. *Environmental Science & Technology* **53**, 7215–7233.

Wang, S., Zhu, B., Liu, M., Zhang, L., Yu, J. & Zhou, M. 2019a Direct Z-scheme ZnO/CdS hierarchical photocatalyst for enhanced photocatalytic H_2-production activity. *Applied Catalysis B-Environmental* **243**, 19–26.

Wang, S., Li, Z., Guan, Y., Lu, L., Shi, Z., Weng, P., Yan, S. & Zou, Z. 2019b Visible light driven $TaON/V_2O_5$ heterojunction photocatalyst for deep elimination of volatile-aromatic compounds. *Applied Catalysis B-Environmental* **245**, 220–226.

Wang, Z., Chen, M., Huang, D., Zeng, G., Xu, P., Zhou, C., Lai, C., Wang, H., Cheng, M. & Wang, W. 2019c Multiply structural optimized strategies for bismuth oxyhalide photocatalysis and their environmental application. *Chemical Engineering Journal* **374**, 1025–1045.

Xu, Z. F., Hao, W. C., Zhang, Q. F., Fu, Z. H., Feng, H. F., Du, Y. & Dou, S. X. 2016 Indirect-direct band transformation of few-layer BiOCl under biaxial strain. *The Journal of Physical Chemistry C* **120**, 8589–8594.

Xu, H. Y., Han, X., Tan, Q., Wu, K. J. & Qi, S. Y. 2017a Crystal-chemistry insight into the photocatalytic activity of $BiOCl_xBr_{1-x}$ nanoplate solid solutions. *Frontiers of Materials Science* **11**, 120–129.

Xu, H. Y., Han, X., Tan, Q., He, X. L. & Qi, S. Y. 2017b Structure-dependent photocatalytic performance of $BiOBr_xI_{1-x}$ nanoplate solid solutions. *Catalysts* **7**, 153.

Yang, C. Y., Li, F., Zhang, M., Li, T. H. & Cao, W. 2016 Preparation and first-principles study for electronic structures of BiOI/BiOCl composites with highly improved photocatalytic and adsorption performances. *Journal of Molecular Catalysis A-Chemical* **423**, 1–11.

Yuan, Y. J., Shen, Z., Wu, S., Su, Y., Pei, L., Ji, Z., Ding, M., Bai, W., Chen, Y., Yu, Z. T. & Zou, Z. 2019 Liquid exfoliation of

Downloaded from http://iwaponline.com/wst/article-pdf/81/5/1080/768292/wst081051080.pdf
by guest

g-C_3N_4 nanosheets to construct 2D-2D MoS_2/g-C_3N_4 photocatalyst for enhanced photocatalytic H_2 production activity. *Applied Catalysis B-Environmental* **246**, 120–128.

Zhang, X., Wang, L. W., Wang, C. Y., Wang, W. K., Chen, Y. L., Huang, Y. X., Li, W. W., Feng, Y. J. & Yu, H. Q. 2015 Synthesis of $BiOCl_xBr_{1-x}$ nanoplate solid solutions as a robust photocatalyst with tunable band structure. *Chemistry-A European Journal* **21**, 11872–11877.

Zhang, X., Wang, C. Y., Wang, L. W., Huang, G. X., Wang, W. K. & Yu, H. Q. 2016 Fabrication of $BiOBr_xI_{1-x}$ photocatalysts with tunable visible light catalytic activity by modulating band structures. *Scientific Reports* **6**, 22800.

First received 13 February 2020; accepted in revised form 19 April 2020. Available online 28 April 2020

Downloaded from http://iwaponline.com/wst/article-pdf/81/5/1080/768292/wst081051080.pdf
by guest